Structure of Human Pro-Chymase: A Model for the Activating Transition of Granule-Associated Proteases[†,‡]

K. Kinkead Reiling,[§,||] Jolanta Krucinski,[§] Larry J. W. Miercke,[§] Wilfred W. Raymond,[⊥] George H. Caughey,[⊥] and Robert M. Stroud*[,§]

Departments of Biochemistry and Biophysics and of Pharmaceutical Chemistry, Graduate Group in Biophysics, and Cardiovascular Research Institute and Department of Medicine, Box 0911, University of California at San Francisco, San Francisco, California 94143

Received September 23, 2002; Revised Manuscript Received January 2, 2003

ABSTRACT: Human chymase is a protease involved in physiological processes ranging from inflammation to hypertension. As are all proteases of the trypsin fold, chymase is synthesized as an inactive "zymogen" with an N-terminal pro region that prevents the transition of the zymogen to an activated conformation. The 1.8 Å structure of pro-chymase, reported here, is the first zymogen with a dipeptide pro region (glycine-glutamate) to be characterized at atomic resolution. Three segments of the pro-chymase structure differ from that of the activated enzyme: the N-terminus (Gly14−Gly19), the autolysis loop (Gly142−Thr154), and the 180s loop (Pro185A−Asp194). The four N-terminal residues (Gly14-Glu15-Ile16-Ile17) are disordered. The autolysis loop occupies a position up to 10 Å closer to the active site than is seen in the activated enzyme, thereby forming a hydrogen bond with the catalytic residue Ser195 and occluding the S1′ binding pocket. Nevertheless, the catalytic triad (Asp102-His57-Ser195) is arrayed in a geometry close to that seen in activated chymase (all atom rmsd of 0.52 Å). The 180s loop of pro-chymase is, on average, 4 Å removed from its conformation in the activated enzyme. This conformation disconnects the oxyanion hole (the amides of Gly193 and Ser195) from the active site and positions only ∼35% of the S1−S3 binding pockets in the active conformation. The backbone of residue Asp194 is rotated 180° when compared to its conformation in the activated enzyme, allowing a hydrogen bond between the main-chain amide of residue Trp141 and the carboxylate of Asp194. The side chains of residues Phe191 and Lys192 of pro-chymase fill the Ile16 binding pocket and the base of the S1 binding pocket, respectively. The zymogen positioning of both the 180s and autolysis loops are synergistic structural elements that appear to prevent premature proteolysis by chymase and, quite possibly, by other dipeptide zymogens.

Proteolytic enzymes are translated as inactive precursors or "zymogens" to prevent inappropriate proteolysis. Inhibitory domains or "pro regions" are cotranslated elements that prevent activation of a protease. These molecular self-inhibitors range in size from fully folded domains rivaling the size of the activated protease to simple dipeptides. Many proteases packaged for secretion, including all chymases (*2*), cathepsin G (*3*), and granzymes B−F (*4*), have dipeptide pro regions composed of a glycine/glutamate and a glutamate attached to the N-terminus of the enzymes. Zymogen activation proceeds via proteolytic removal of the pro region. Trypsin, for example, is usually activated by enterokinase (*5*), and chymase is activated in trans by dipeptidyl peptidase I (DPPI)[1] (*6*).

A structural mechanism by which pro regions compromise the catalytic potency of their cognate proteases is to prevent the proper folding of the proteolytic machinery (reviewed in ref *7*). In the zymogens of trypsin-like proteases, the oxyanion hole (the amides of Gly193 and Ser195) and ∼50% of the substrate binding pockets are not in the catalytically competent conformation seen in the activated enzyme. For instance, in chymotrypsinogen components of the S1, S2, and S3 binding sites are several angstroms removed from their conformation in the activated enzyme (*8*, *9*). Trypsinogen presents S1−S3 binding sites that are distorted and somewhat disordered with respect to active trypsin (*10*, *11*). The zymogen of the protease tissue-type plasminogen activator has a substrate binding site and oxyanion hole almost identical to that of the activated enzyme and a corresponding activity only 10-fold below that of the activated enzyme (*12*). In contrast to these conformational changes, the catalytic triad

[†] Research supported by Grant R01 CA6308-06A1 (R.M.S.) and NIH Grant HL24136 (G.H.C. and W.W.R.). Graduate fellowship support was provided by NIH Graduate Training Grant GM08204 (K.K.R.) and an ARCS Foundation grant (K.K.R.).

[‡] Coordinates have been deposited in the Brookhaven Protein Data Bank: 1NN6.

* To whom correspondence should be addressed. Telephone: (415) 476-4224. Fax: (415) 476-1902. E-mail: stroud@msg.ucsf.edu.

[§] Departments of Biochemistry and Biophysics and of Pharmaceutical Chemistry.

[||] Graduate Group in Biophysics.

[⊥] Cardiovascular Research Institute and Department of Medicine.

[1] Abbreviations: DPPI, dipeptidyl peptidase I; ACE, angiotensin converting enzyme; PMSF, phenylmethanesulfonyl fluoride; CMK, chloromethyl ketone; rmsd, root-mean-squared deviation; "autolysis loop", residues Gly142 to Thr154 of pro-chymase; "180s loop," residues Pro185A to Asp194 of pro-chymase. (P3, P2, P1) and (P1', P2', P3') refer the inhibitor residues N-terminal and C-terminal of the scissile peptide bond, respectively; (S3, S2, S1) and (S1', S2', S3') correspond inhibitor binding pockets on the protease (*1*).

10.1021/bi020594d CCC: $25.00
Published on Web 02/11/2003

(Asp-His-Ser) of zymogens is arrayed as seen in the activated enzyme. Despite possessing a common activated conformation constrained by the chemistry they perform, different proteases adopt unique, inactive zymogen conformations.

In each case, proteolytic processing of trypsin-like enzymes severs the pro region from the parent enzyme to liberate a highly conserved N-terminus (I-I/V-G-G). Binding of the two N-terminal residues of the activated enzyme in an "activation pocket" establishes a conserved and buried salt bridge between the newly formed amino terminus and Asp194 (chymotrypsin numbering is used throughout). The conformational change that accompanies and allows this salt bridge repacks approximately 10% of the molecule and ushers the remainder of the protein into the conformation required for catalysis (*5*, *8*−*11*). An understanding of the unique aspects of a zymogen structure can shed light upon the activating transition and the determinants of activity for each enzyme.

We present here the 1.8 Å structure of the zymogen of human chymase. Human chymase is the major non-angiotensin converting enzyme (ACE), angiotensin II-generating enzyme in human tissues (*13*−*15*). Multiple studies cite chymase activity as a contributor to ACE-resistant ventricular hypertrophy (*16*), vascular restenosis (*17*, *18*), and hypertension (*19*−*21*). The structure of pro-chymase is compared to two previously determined structures of activated chymase to identify the determinants of inactivity of the zymogen. A model for chymase activation is presented and interpreted in the context of the structural models for the activating transition of other trypsin-like zymogens.

EXPERIMENTAL PROCEDURES

Cloning, Protein Purification, and Activity Assay. For studies of human pro-chymase, we generated pro-chymase in insect cells as described previously (*22*). Briefly, human chymase cDNA encoding the full pre-pro-enzyme was obtained by PCR from human lung cDNA (Clontech, Palo Alto, CA) using primers based on the Caughey laboratory's previously determined gene sequence (*2*). The pre-pro-chymase cDNA was ligated into the baculovirus transfer vector pVL1392 (Pharmingen, San Diego, CA), which was cotransfected with linearized wild-type baculovirus DNA into Sf9 (*Spodoptera frugiperda*) cells (Invitrogen, Carlsbad, CA) to generate recombinant virus. High Five (*Trichoplusia ni*) cells (Invitrogen) infected with recombinant virus yielded supernatants containing pro-chymase, which was purified by heparin affinity chromatography on a heparin 5PW column (Toso-Haas, Montgomeryville, PA). A linear gradient of 0.4−2 M NaCl in 10 mM Bis-Tris-HCl (pH 6.1) was applied to the column, with pro-chymase eluting at 1.4 M NaCl. N-Terminal sequencing and SDS−PAGE electrophoresis were used to confirm the identity and purity of recombinant pro-chymase. The proteolytic activity of recombinant pro-chymase against the substrate succinyl-L-Ala-Ala-Pro-Phe-4-nitroanilide was measured under the assay conditions described by Caughey et al. (*22*): 1 mM succ-AAPF-pNA in 0.45 M Tris, pH 8, 1.8 M NaCl, and 9% DMSO at 25 °C.

Protein Concentration and Crystal Growth. After purification, protein was dialyzed against buffer composed of 500 mM NaCl and 2 mM Bis-Tris (pH 6.1) and then concentrated to 5.0 mg/mL. Crystals of pro-chymase were grown by hanging drop vapor diffusion. Pro-chymase crystallized in drops composed of a mixture of 2 μL of well buffer and 2 μL of protease solution. Droplets were equilibrated against 1 mL of crystallization well buffer composed of 20% PEG 4K, 150 mM sodium formate, and 100 mM Tris (pH 8.5). Plates were set up at 4 °C in November of 1997, and crystals were first noted in drops in February of 1999. The crystal belonged to space group $P2_12_12_1$ with unit cell dimensions of $a = 50$ Å, $b = 56$ Å, and $c = 89$ Å.

Data Collection and Refinement. The structure was refined against a 1.8 Å data set collected at SSRL beam line 9-1 using a crystal frozen in mother liquor supplemented with 15% glycerol. A total of 120 frames, each traversing 0.75 deg about the ϕ-axis, were collected. Diffraction data were integrated, scaled, and merged using the HKL package (*23*). The structure was determined by molecular replacement methods starting with a model of activated human chymase [1KLT (*24*)] in which the side chains were all changed to serines as the search model for the program AMoRe (*25*) of the CCP4 suite (*26*). Data from 10 to 3.0 Å yielded a post-rigid-body refinement R factor of 47.5% and correlation coefficient of 57.9%. Initial $2F_o - F_c$ and $F_o - F_c$ maps, phased using the polyserine model, indicated a movement of the 30s loop (35−42), the autolysis loop[2] (144−155), and the 180s loops. No density corresponding to the N-terminus was discernible. Residues 16−19, 144−155, and 187−196 were removed from the polyserine model. This trimmed model was adjusted to match difference density and then entered into multiple cycles of simulated annealing followed by sequential positional and temperature factor refinement using CNS (*27*). Intervening cycles of manual model rebuilding used the MOLOC (*28*) and QUANTA graphical interfaces. With the exception of the N-terminus, residue Lys188, and residue Ser189, all initially removed loops where reinterpreted as refinement progressed. As refinement converged, the model was ported to REFMAC5 (*29*) of the CCP4 package to allow simultaneous refinement of individual atomic positions and temperature factors and facile introduction of multiple side-chain conformations. The final model was refined to crystallographic R factors of 20.3% and 24.5% (working, free; Table 1). The model contains all residues of pro-chymase with the exception of residues Gly14, Glu15, Ile16, Ile17, Lys190, and Ser191. Residues Ser38, Arg51, and Thr67 exhibit multiple side-chain conformations. Some atoms for the side chains of residues Glu21, Lys43, Lys89, Gln128, Leu149, Lys150, Gln167, Arg173, Arg187, Lys188, and Lys219 were not visible in the electron density.

Structural Comparison. Structure alignments were carried out by the method of least-squares superposition as implemented in LSQMAN of the O suite (*30*). For alignment to either phenylmethanesulfonyl fluoride treated (PMSF-chymase) [1KLT (*24*)] or the chloromethyl ketone, tetrapeptide (Ala-Ala-Pro-Phe) inhibited (AAPF-CMK-chymase) [1PJP (*31*)], an invariant core was derived from analysis of difference distance matrices produced using an in-house algorithm; core residues are 43−98, 100−120, 160−183, and 198−241. On the basis of this alignment, the substrate

[2] Loop Gly142 to Thr154 is deemed the "autolysis loop" in reference to the fact that the corresponding loop in β-trypsin and α-chymotrypsin is autolytically cleaved.

Table 1: Statistics on Diffraction Data and Final Model

data reduction resolution range (Å)	28.7−1.75
average $I/\sigma(I)$	26.8 (1.7)[a]
no. of observations	222007
unique structure factors	27938
space group	$P2_12_12_1$
unit cell dimensions (Å)	
a	50.1
b	55.6
c	88.7
R_{merge} (%)[b]	4 (69)
completeness (%)	98.3 (97.5)
mosaicity (deg)	0.61
Wilson *B* factor (Å^2)	30.1
solvent content (%)	42
refinement residuals [working/free (%)]	20.3/24.5
no. of residues	222
no. of non-hydrogen atoms	
protein	1708
waters	156
sugars (3 × NAG)	42
deviation from ideality (rmsd)	
bond distances (Å)	0.017
angles (deg)	1.8

[a] Values in parentheses represent the highest resolution bin (1.77−1.75 Å). [b] $R_{merge} = \sum|I - \langle I\rangle|/\sum|\langle I\rangle|$.

present in the AAPF-CMK-chymase structure was superimposed onto the pro-chymase structure. The interactions of AAPF-CMK-chymase with its crystallographically determined inhibitor and of pro-chymase with the modeled inhibitor were annotated utilizing the Web-based Ligand-Protein Contacts software (http://bioinfo.weizmann.ac.il:8500/oca-bin/lpccsu). The volumes of surface pockets were calculated utilizing the Web-based program CAST (http://cast.engr.uic.edu/cast/) (*32*).

RESULTS

Overall Fold. Pro-chymase exhibits the canonical trypsin fold comprised of two, six-stranded β-barrels. Three crossing strands link the two β-barrels (Figure 1): the N- and C-termini and the Glu110−Gly133 loop. Pro-chymase is glycosylated at residues Asn79 and Asn97, and the attached sugars are modeled as *N*-acetyl-D-glucosamine (NAG) moieties (Table 1). In this study, the structure of pro-chymase is compared to both the PMSF-chymase [1KLT (*24*)] and the AAPF-CMK-chymase [1PJP (*31*)] structures of activated chymase. The two, independently determined structures of activated chymase align with each other with a Cα rmsd of 1.0 Å and an all-atom rmsd of 1.6 Å. Optimal structural superposition of pro-chymase with AAPF-CMK-chymase yields a Cα rmsd of 0.5 Å and an all-atom rmsd of 2.1 Å for the enzyme core (defined in Experimental Procedures) and a 2.0 Å Cα rmsd and an all-atom rmsd of 2.3 Å for all residues.

Five regions of pro-chymase diverge from the structure of both activated chymases (Figures 1 and 2). The movement of the autolysis loop (Gly142−Thr154), the 180s loop (Pro185A−Asp194), and the N-terminus (Gly14−Gly19) appears to relate directly to the inactivity of pro-chymase. The 30s loop (Ser36B−Ser39) is positioned up to 5 Å away from its position in AAPF-CMK-chymase. This difference appears to result from the placement of the autolysis loop and crystal contacts at residues Asn36C and Pro38 in pro-chymase. Finally, the 120s β-barrel linker loop (Glu110−Gly133) varies among the activated chymase structures, and thus its variability may reflect inherent flexibility unrelated to the inactivity of pro-chymase.

The N-Terminus and the Ile16 Binding Pocket. In pro-chymase, the pro region (Gly14-Glu15) and the N-terminus of the mature enzyme (Ile16-Ile17) are not interpretable in the electron density maps. Residues Gly18 and Gly19 lie within weak density in this region of the $2F_o - F_c$ maps (Figure 3). Definitive electron density begins at residue Thr20, which is shifted toward solvent and away from the protein core by 1.5 Å as compared to the activated enzyme. In AAPF-CMK-chymase and PMSF-chymase, the N-terminus (Ile16-Ile17) interacts with the 180s loop, the autolysis loop, and a pocket formed by residues Val138-Ala139-Gly140 and Val158-Glu157-Gln156 of strands 1 and 2 of the C-terminal β-barrel. The N-terminal amide of residue Ile16 forms hydrogen bonds with the carboxylate group of residue Asp194 and the carbonyl of residue Arg143.

In pro-chymase, residue Asp194 rotates approximately 180° to form a hydrogen bond with the backbone amide of residue Trp141 (Figure 3). The zymogen backbone geometry of residue Asp194 is strained, having a backbone ω angle and a Cα chirality (165° and 41°, respectively) that are 2σ from the ideal values. In chymotrypsinogen, residue His40 of the 30s loop forms a hydrogen bond with Asp194 and has been postulated to stabilize the zymogen conformation of the 180s loop [1CHG (*8*)] (*33*, *34*). In pro-chymase, Lys40 is rotated 180° and translated by 5.5 Å relative to trypsinogen [1TGN (*10*), 1TGB (*11*)] or chymotrypsinogen [1CHG (*8*), 2CGA (*9*)] and is unavailable to affect the conformation of Asp194. In pro-chymase, residue Asp194 is not situated in the conformation that forms a salt bridge with the N-terminal NH_3^+ of Ile16 in the activated enzyme and, instead, is rotated and is stabilized in the zymogen conformation by a buried hydrogen bond with Trp141 and not with residue 40.

The conformational difference beginning at residue Asp194 extends back to residue Pro185A and results in an average displacement of 4 Å for the 180s loop from the conformation seen in the AAPF-CMK-chymase structure (Figure 4). The zymogen conformation of the 180s loop in pro-chymase occludes the Ile16 binding pocket, filling all but 14 Å^3 of the 273 Å^3 cavity that forms upon binding of the mature N-terminus (Ile16-Ile17). In pro-chymase, the side chain of residue Phe191 fills the space where residue Ile16 will insert upon enzyme activation and is related to its conformation in AAPF-CMK-chymase by a 5.4 Å translation and a 90° rotation. Residue Lys192 of pro-chymase is situated within the S1 binding pocket (Figure 4). Residues Lys188 and Ser189 are not visible in the electron density maps. In the activated enzyme, residue Ser189 sits at the base of the S1 binding pocket. The protein chain is again traceable at residue Thr187, but strong density for both main- and side-chain atoms is not evident until residue Pro185A. The backbone conformation for the 180s loop of pro-chymase is in an extended conformation that is removed from the substrate binding pockets.

The Incompletely Formed S3−S1 Binding Pockets of Pro-Chymase. The binding determinants and transition state stabilization elements of activated chymase are only partially formed in pro-chymase. The catalytic triad of pro-chymase (Asp102-His57-Ser195) aligns with that of the activated

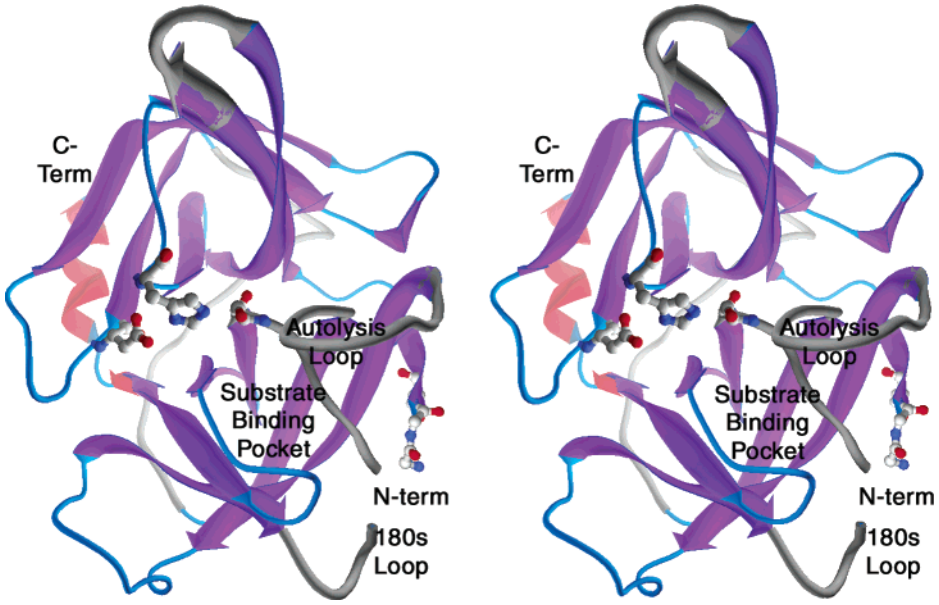

FIGURE 1: The fold of pro-chymase. Depicted in this figure is a cross-eyed stereo, ribbon representation of the structure of pro-chymase. The active site residues (Asp102, His57, and Ser195) along with the N-terminus (Gly18 and Gly19) are rendered as ball and stick. The regions of pro-chymase that differ from AAPF-CMK- and PMSF-chymase are colored gray and rendered with twice the thickness of all other loops. The sheets, loops, and helices of the invariant regions of pro-chymase are colored purple, light blue, and red, respectively. The figure was produced using the programs SwissPDBviewer (*45*) and POVray.

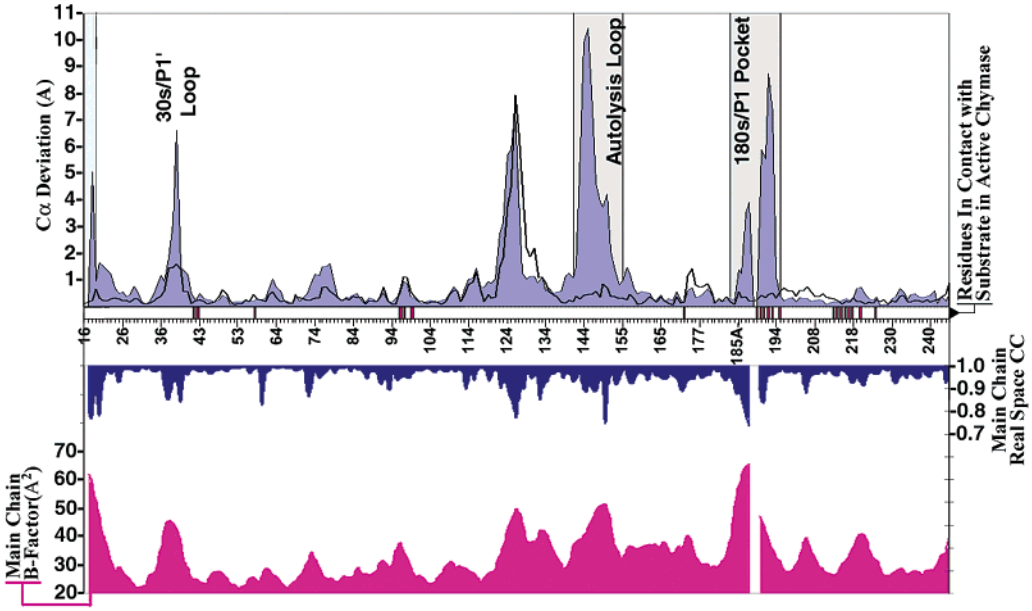

FIGURE 2: Conformational change upon activation and structural figure of merit of the pro-chymase structure. The upper graph is the Cα deviation (Å) of the AAPF-CMK-chymase structure from the pro-chymase structure (blue area graph) and of the AAPF-CMK-chymase structure from the PMSF-chymase (black line). For both comparisons, the structures were aligned as described in the Experimental Procedures. The lower graph is an overlay of the average *B* factor (pink, lower half, left axis) and of the real space correlation coefficient between electron density and atom positions (blue, upper half, right axis) for the main-chain atoms of each residue of pro-chymase. The *X*-axis is residue numbers using chymotrypsinogen numbering. The small central graph is a binary indicator of contacts between the protease and the inhibitor in the AAPF-CMK-chymase structure. Real space correlation coefficients were calculated using the CCP4 (*26*) programs SFALL, FFT, and OVERLAPMAP.

enzyme (AAPF-CMK-chymase) with an all-atom rmsd of 0.4 Å (Figure 3). The position of residue Ser214 and the stabilizing hydrogen bond it makes with residue Asp102 are also preformed in pro-chymase (2.8 and 2.6 Å in pro-chymase and AAPF-CMK-chymase, respectively). The amide of Gly193, a component of the oxyanion hole, is not properly arrayed for catalysis due to a 7.6 Å translation and 180° rotation. In the AAPF-CMK-chymase structure, residues Ser189−Ser195, Val213−Ser218, Ala220, and Ala226 define the S1−S3 binding pockets. The conformation of the 180s loop in pro-chymase leaves unformed ∼75% (647 vs 155 Å^2), ∼15% (72 vs 63 Å^2), and ∼15% (81 vs 70 Å^2) of the S1, S2, and S3 pockets, respectively (Figure 5). In contrast, residues Ser214−Gly216 of pro-chymase form a β-strand, which is arrayed as is seen in the activated chymase structures. Residue Gln236, from a symmetry-related molecule, interacts with the P3 pocket (214−216) and may stabilize the activated conformation of the loop. The

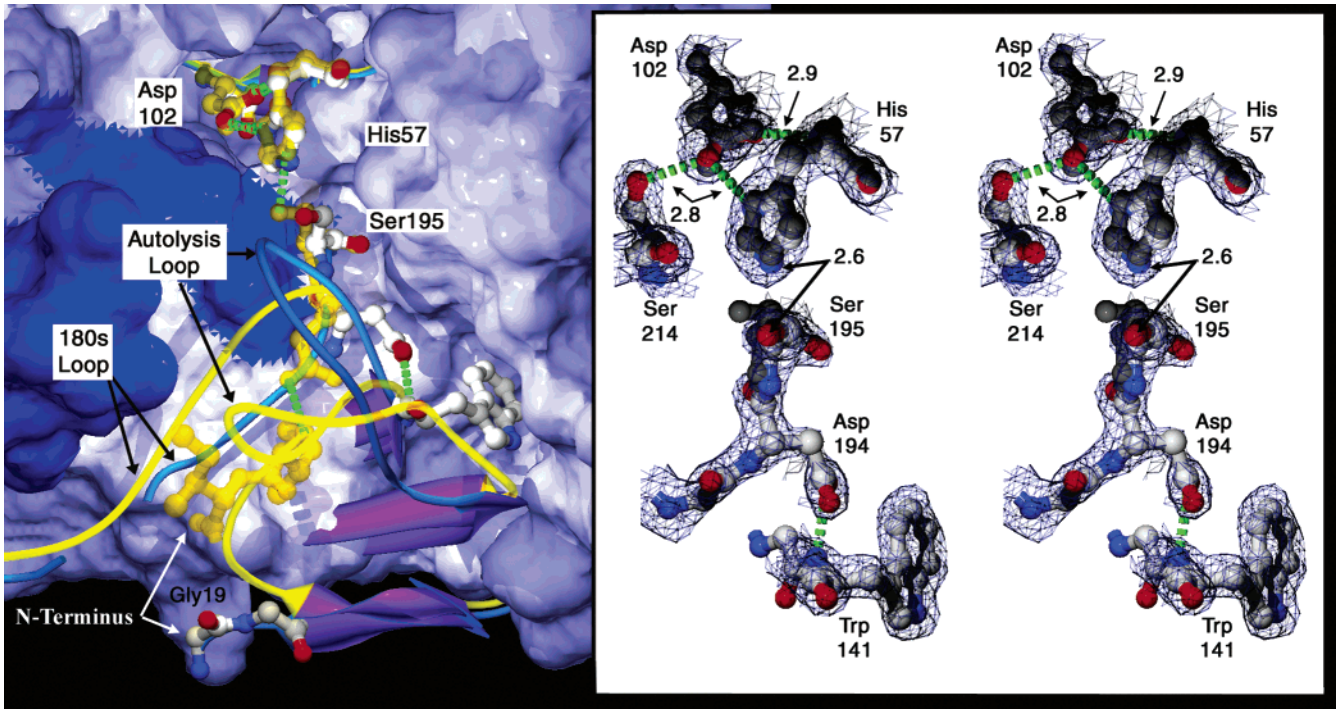

FIGURE 3: Positioning of the catalytic triad and residue Asp194 in pro-chymase. (Left) In semitransparent yellow are the catalytic triad (top center of figure, residues Asp102, His57, and Ser195), the 180s loop, the autolysis loop, and the N-terminus of the AAPF-CMK-chymase structure. The catalytic triad and residues Asp194, Trp141, Gly18, and Gly19 of pro-chymase are shown in solid CPK. Shown in the center of the image is the activation-induced conformational change of Asp194, which interacts with Trp141 in pro-chymase (solid CPK) and forms a salt bridge with the mature N-terminus in the activated enzyme (semitransparent yellow). The surface is that of pro-chymase with the autolysis loop, the 180s loop, and the catalytic triad omitted from the surface calculation. The darker blue section of the surface is the 220s loop, which is unchanged between AAPF-CMK-chymase and pro-chymase. (Stereo box) Rendered in ball and stick and overlaid upon each other are the catalytic triads of AAPF-CMK-chymase (dark gray) and pro-chymase (CPK coloring). Residue Ser214 of pro-chymase is shown along with the complement of active site hydrogen bonds for pro-chymase. The Asp194−Trp141 interaction is once again shown. All residues are depicted in 1σ $2F_o - F_c$ omit map electron density. The figure was produced using the programs SwissPDBviewer (*45*) and POVray.

Val213−Ala226 loop has a two-residue deletion relative to chymotrypsinogen and contains a *cis*-proline (220−221), which may rigidify the loop. In other trypsin-like enzymes, a disulfide bond between residues Cys191 and Cys220 links the two substrate binding pocket-forming loops. In the context of the pro-chymase structure, this loss of connectivity decouples, to some extent, the conformation of the Val213−Ala226 loop from that of the 180s loop. In pro-chymase, the S1−S3 binding pockets and the transition state stabilizing elements are not in a catalytically competent conformation.

The Autolysis Loop. The autolysis loop (Gly142−Thr154) of pro-chymase binds across the S1 and S1′ substrate binding pockets and forms a hydrogen bond with the catalytic triad member Ser195. In both the activated and the zymogen conformations, the conserved stacking pair Trp141-Leu155 is similarly positioned at the base of the autolysis loop. In the activated enzyme, residue Val146 extends across the N-terminus to interact with the backbone of residue Asp219, closing the autolysis loop down on top of the mature N-terminus. The remainder of the autolysis loop protrudes into solvent. This is not the case in pro-chymase, where the autolysis loop is positioned in the active site of the enzyme up to 10 Å away from the activated conformation. In pro-chymase, the side chain of residue Arg143 is situated in the S1' pocket and related to the activated conformation by a 120° rotation and a 5.8 Å translation. This placement of residue Arg143 would clash with the side chain of residue Phe41, as seen in AAPF-CMK-chymase, if not for a 132° rotation of residue Phe41 about χ_1 in pro-chymase (Figure 6). The side chain of residue Thr144 of pro-chymase occupies the volume in which the backbone atoms of residues Asp194 and Gly193 are positioned in the activated chymase structures (Figure 4). From this position, the hydroxyl of residue Thr144 makes a 2.7 Å hydrogen bond with the hydroxyl of residue Ser195. To confirm the unique position of the autolysis loop in pro-chymase, a $2F_o - F_c$ omit map was examined. In this map, the autolysis loop backbone atoms exhibit contiguous density for all residues except Gly142 (Figure 6). It must be noted that residue Val146 of pro-chymase is involved in a crystal contact, which may partially stabilize the loop in its occlusive conformation. In addition to blocking the S1′ pocket and filling the space to be occupied by the oxyanion hole in the activated enzyme, the zymogen conformation of the autolysis loop enlarges the Ile16 pocket, which accommodates the placement of residue Phe191.

DISCUSSION

Interactions among the loops bordering and defining the active site appear to influence both the zymogen and the activated conformations of chymase. These structural differences between activated and pro-chymase translate into a ~7000-fold increase in activity upon activation: the specific activity of pro-chymase is 1.1×10^{-2} μmol min^{-1} (mg of enzyme)$^{-1}$ (reported here) vs 77 μmol min^{-1} mg^{-1} for the activated enzyme (*22*).

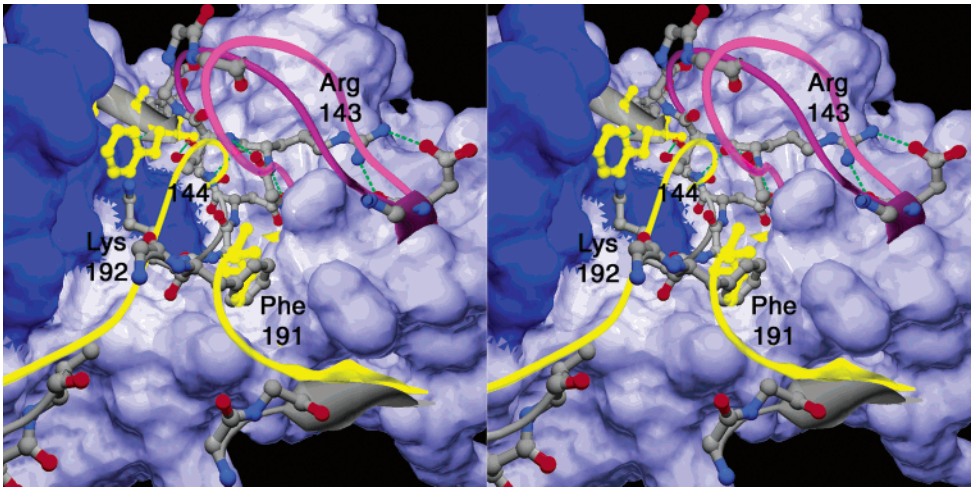

FIGURE 4: Occlusion of the Ile16 pocket. The 180s loop, substrate, and N-terminus as arrayed in AAPF-CMK-chymase are depicted semitransparently in yellow. Depicted in gray are the 180s loop, the N-terminus, and select residues of the autolysis loop of pro-chymase. The conformations of the autolysis loop in both pro-chymase (dark magenta) and AAPF-CMK-chymase (lighter magenta and closer) are also shown. The surface is of pro-chymase with the 180s loop, the autolysis loop, and the N-terminus omitted from the surface calculation. The darker blue section of the surface is attributable to the 220s loop, which is unchanged between AAPF-CMK-chymase and pro-chymase. Depicted in the figure is residue Phe192 of pro-chymase in the pocket into which the mature N-terminus of the activated enzyme will bind. The placement of residues Lys192 and Thr144 of pro-chymase within the S1 binding pocket or occupying the space in which the oxyanion hole will move upon activation is shown. The figure was produced using the programs SwissPDBviewer (*45*) and POVray. Two movies illustrating the conformational change from pro-chymase to activated chymase are available at the following webpage: www.msg.ucsf.edu/stroud/index.html. These movies were made by structural interpellation between the AAPF-CMK-chymase and pro-chymase structures utilizing the programs rigimol and PyMOL (DeLano Scientific) and not experimentally derived structural intermediates. PDB files and a PyMOL script are also available for interactive exploration of the activation of pro-chymase.

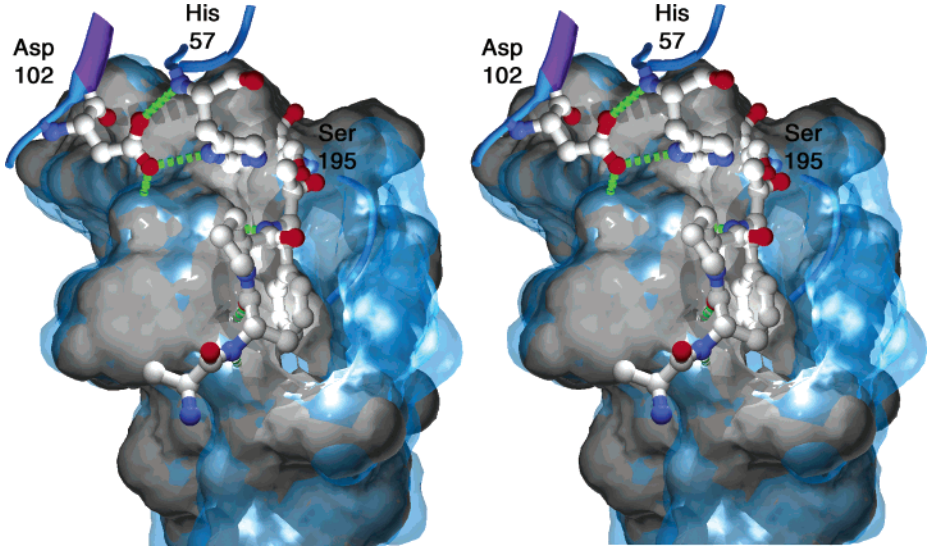

FIGURE 5: Approximately one-half of the S3−S1 binding pockets are not formed in pro-chymase. P4−P1 of the substrate from AAPF-CMK-chymase is shown in ball and stick superimposed on the catalytic triad of pro-chymase. In gray are the substrate binding pockets of pro-chymase, which are formed by the 220s and 180s loops. In light blue and rendered semitransparently is the surface for the same loops of AAPF-CMK-chymase. A ribbon backbone for the AAPF-CMK-chymase 180s loop is shown beneath the light blue surface. The figure was produced using the programs SwissPDBviewer (*45*) and POVray.

180s Loop. The positioning of the 180s loop in pro-chymase situates residue Lys192 within the S1 substrate binding pocket and residue Phe191 within the hydrophobic cleft that will accept the mature N-terminus (Ile16 binding pocket; Figure 4). In chymotrypsinogen, residue Met192 fills the Ile16 binding pocket and residue 191 is a cysteine, which forms a disulfide bond with Cys220 [1CHG (*8*), 2CGA (*9*)]. Absence of this disulfide, concurrent with a shortening of the 220s loop, is a sequence hallmark of the granule-associated protease, such as chymase (*35*). In these dipeptide zymogens, residue 191 tends to be a large hydrophobic: phenylalanine or tyrosine. Either of these amino acids could substitute for residue Ile16 in the N-terminal binding pocket as seen in pro-chymase. Among the dipeptide zymogens, residue 192 is most often a lysine but is also seen as other amino acids. Also positioned at the base of the S1 pocket, residue 226, an alanine in chymase, is the primary specificity determinant of some granule proteases. Granzyme B [1IAU (*36*) and 1FI8 (*37*)] and cathepsin G [1CGH (*38*)] have an arginine or glutamate at residue 226, respectively. Although each enzyme still exhibits a large, charged residue at 192 (arginine for granzyme B and lysine for cathepsin G), a positioning of residue 192 at the base of the S1 pocket in the zymogens of granzyme B and cathepsin G would be

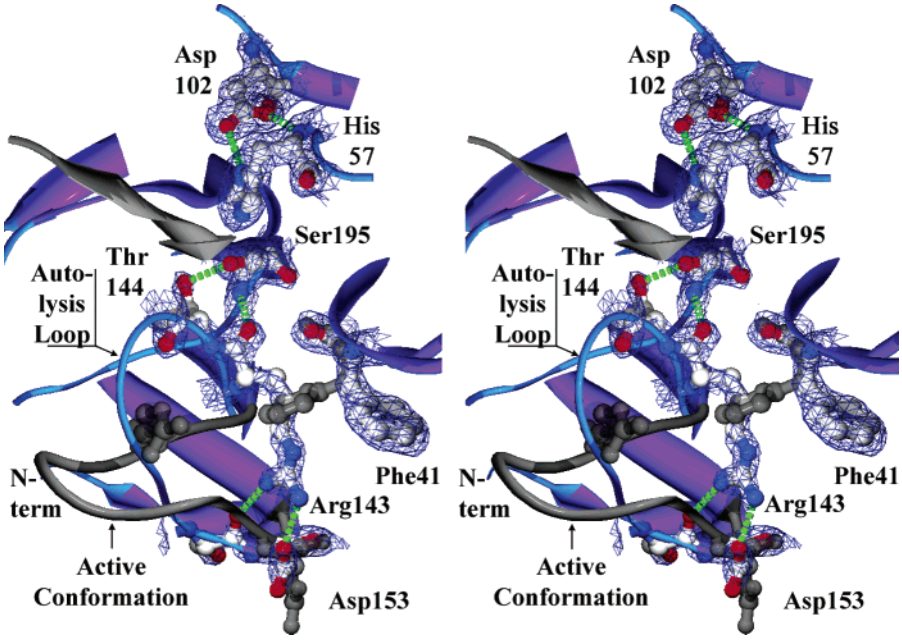

FIGURE 6: The autolysis loop occludes the S1 and S1′ pockets of pro-chymase. The autolysis loop of pro-chymase is up to 10 Å closer to the active site than it is in AAPF-CMK-chymase. The activated and zymogen conformations for residues Arg143, Phe41, and Asp153 are shown. The catalytic triad of pro-chymase hydrogen bonding to Thr144 is represented in ball and stick and colored according to CPK. Regions of pro-chymase surrounding the autolysis loop are depicted in purple ribbons and thin blue tubes. The autolysis loop and substrate of the AAPF-CMK-chymase structure are depicted in gray (either CPK, as a thick tube for the autolysis loop, or as a sheet for the substrate). Electron density encasing the figure is a $2F_o - F_c$ omit map contoured at 1σ. The figure was produced using the programs SwissPDBviewer (*45*) and POVray.

incompatible with the conformation of residue 226 as seen in the activated enzymes. Sequence conservation among the dipeptide zymogens suggests that a positioning of residue 192 within the S1 binding pocket and a substitution of residue 191 for the N-terminus in the Ile16 binding pocket may be common but not universal contributors to the inactivation of dipeptide zymogens.

The Autolysis Loop. The autolysis loop appears to contribute to the active site conformation of both the active and inactive forms of chymase. In the activated enzyme, the autolysis loop (Gly142−Thr154) extends over the N-terminus to interact with the two activation domain loops (residues 191−194 and 218−221) that define the S1−S4 binding pockets. In pro-chymase, the autolysis loop interacts with the 180s loop and the prime-side substrate binding pockets. Thr144 of the autolysis loop forms a hydrogen bond with Oγ of residue Ser195 and occupies the space into which the oxyanion hole will move upon chymase activation. Structural investigation of either trypsinogen [4TPI (*39*)] or chymotrypsinogen [1CGI (*40*)] bound to a macromolecular inhibitor indicates that the interactions among the three active site loops are not dependent solely upon the binding of the N-terminus. The autolysis loops in the trypsinogen and chymotrypsinogen structures adopt the activated conformation with minimal contact to the inhibitor (Tyr151 of trypsinogen with Arg17 and Val34 of bovine pancreatic trypsin inhibitor). Tissue-type plasminogen activator (sc-tPa) is another enzyme in which the autolysis loop is thought to influence the conformation of a zymogen (*12*). Residue His144 of sc-tPa is thought to form a hydrophobic "lid", which shields the Ile16 pocket from solvent and stabilizes a salt bridge between Asp194 and Lys156 (*12*). The autolysis loop appears to both stabilize activated chymase, through interactions with the activation domain, and contribute to the inactivity of pro-chymase by blocking the S1 and S1′ binding pockets. Comparison to other trypsin-like proteases suggests that this dual role for the autolysis loop may not be unique to chymase.

The N-Terminus in Pro-Chymase. A two-residue pro region prevents the activation of pro-chymase. To ask whether this pro region could bind to the Ile16 pocket and form a salt bridge to Asp194, residues Ile16 and Ile17 of the PMSF-chymase structure were modeled as a glycine and a glutamate, respectively. By analogy to studies of trypsinogen in which Ile16 is mutated to a glycine (*41*), the N-terminal glycine of pro-chymase would derive 4−5 kcal/mol less binding affinity than would residue Ile16 with its pocket. When residue Ile17 is modeled as a glutamic acid, the two most common glutamate rotamers do not clash with the surrounding residues. Two glycines follow residues Ile16 and Ile17 and make a tight turn, allowing residue Thr20 and subsequent residues to form a β-sheet with strand 2 of the C-terminal β-barrel. In the context of pro-chymase, binding of residues Gly14 and Glu15 to the N-terminal pocket and the subsequent positioning of Ile16, Ile17, Gly18, and Gly19 may not accommodate the interactions of Thr20 and subsequent residues with the β-barrel as seen in activated chymase. This possible movement of Thr20 derives circumstantial support from the observation that in pro-chymase Thr20 is 1.5 Å removed from its position in PMSF-chymase, due possibly to the altered position of Gly19 and other N-terminal residues in the zymogen. The N-terminus of pro-chymase may be unable to affect the transition to an active conformation due to the loss of hydrophobic interactions for Gly14 versus Ile16 and the disruption of interactions between Thr20 and subsequent residues with the β-barrel.

Activation of Chymase by DPPI. In vivo, in vitro, and genetic studies indicate that removal of the pro region by

DPPI is necessary and sufficient for human chymase activation (*6*). Initial, in vivo studies with recombinant human chymase indicated that the presence of heparin potentiates the activation of chymase by DPPI (*42*). High salt concentrations could not substitute for this heparin effect. The activation-enhancing effect of heparin was abrogated by mutation of the second residue of the pro region (Glu15) to either an alanine or a lysine. On the basis of these data, Murakami et al. proposed a model for the activation of pro-chymase in which the negatively charged N-terminus (Glu15) is sequestered in the zymogen, possibly by the concentration of positively charged residues in the 180s loop (Arg185B, Lys186, Lys188, and Lys192) (*42*). Binding of heparin to specific binding sites would then liberate the N-terminus and grant DPPI access for cleavage. The pro region of pro-chymase, in fact, has no net charge, with the negative charge of Glu15 counterbalanced by the positive charge of the N-terminus. Therefore, there is no reason a priori for the N-terminal pro region to be directed to the concentration of positive residues in the 180s loop. Contrary to the findings of Murakami et al., McEuen et al. found that both heparin and high salt inhibited the activation of pro-chymase by DPPI with equal potency, when adjusted for ionic strength (*43*). In both studies, salt concentrations of greater than 1 M were required to modulate the activation of pro-chymase by DPPI. It is unlikely then that the 150 mM sodium formate in our crystallization buffer would affect the position of the N-terminus in our structure of pro-chymase. The disordered N-terminus in our structure does not support the sequestering model of Murakami et al.

Since activated chymase binds to heparin with greater affinity than pro-chymase (*22*, *44*) and the conformational change in the zymogen is concentrated at the active site, there may exist a heparin binding site proximal to the 180s loop for which the activated conformation of chymase has higher affinity for heparin than the zymogen conformation. The disordered nature of Pro185A−Ser189 in pro-chymase could account for this difference in binding by presenting a poorly ordered site in the zymogen. Analysis of the human DPPI structure reveals that the substrate binding surface is highly electronegative. This charge would complement the electropositive character of chymase (Figure 7). That high ionic strength (salt or heparin) inhibits or screens activation (*43*) is consistent with an electrostatic complementation between DPPI and chymase. Together, these results suggest a physiological model for chymase activation in which, after activation, heparin would promote the dissociation of chymase from DPPI. Further, the higher affinity of activated chymase for heparin proteoglycans may contribute to the preferential packaging of activated chymase into heparin-rich granules in vivo.

CONCLUSION

The zymogens of proteolytic enzymes must be stabilized against inappropriate proteolytic activity. As zymogens initially fold, they form only a portion of the catalytic machinery. The activation domain (Gly142−Pro152, Gly184A−Gly193, and Gly216−Asn223) of the enzymes is stalled en route to proteolytic competence by the absence of the free N-terminus of residue Ile16. Formed by an activating cleavage, the mature N-terminus binds and thus promotes the activated conformation of the enzymes. The conformation

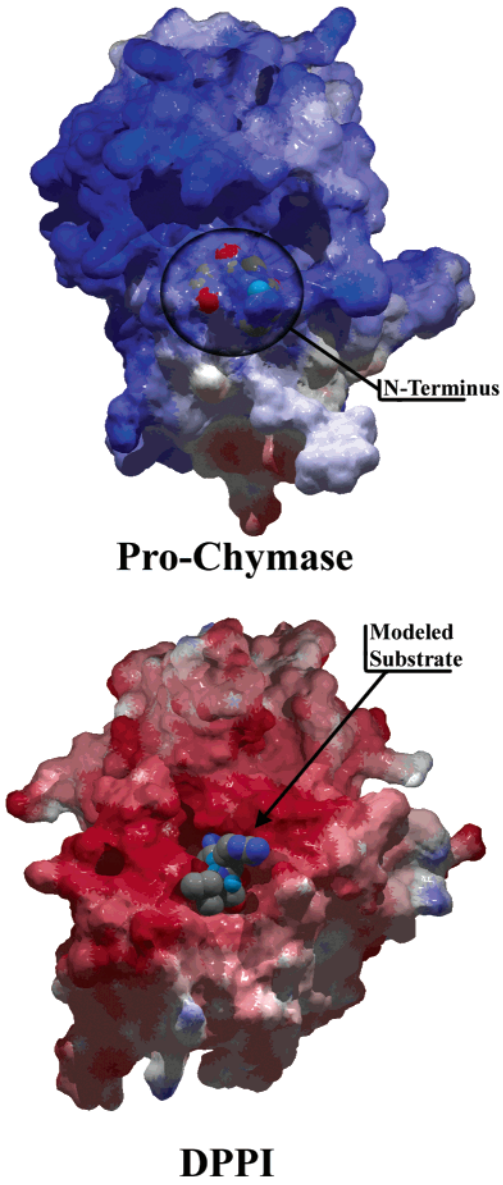

FIGURE 7: Electrostatic complementation of chymase with DPPI. Molecular surfaces for DPPI [1K3B (*46*)], pro-chymase, and AAPF-CMK-chymase are colored by mapping each protein's electrostatic potential to the surface. The electrostatic potentials for the two surfaces are on the same scale. The figure was produced using the programs SwissPDBviewer (*45*) and POVray.

of the activation domain differs among trypsin-like zymogens, but common themes exist; the S3−S1 binding pockets are incompletely formed, and the oxyanion stabilization elements are removed from the active site.

Pro-chymase exhibits many of these features and in addition exhibits a unique positioning of the autolysis loop. The 180s loop is in a conformation that occludes the Ile16 binding pocket and leaves unformed ~60% of the S1−S3 binding pockets. The conformation of the 180s loop in chymase positions residue Lys192 within the S1 binding pocket. The 220s loop is in an activated conformation due possibly to the absence of a disulfide bridge connecting it to the 180s loop, the shortening of the 220s loop as compared to chymotrypsinogen, and the presence of a *cis*-amide bond between residues Pro224 and Pro225. The autolysis loop occupies the position of the oxyanion hole in the activated enzyme and occludes the S1 and S1′ binding pockets. The

two-residue pro region appears not to bind to the Ile16 pocket due to loss of favorable hydrophobic interactions between Gly14 and the Ile16 binding pocket. Further, any binding of the pro region to the activation pocket might result in the loss of interactions between residues Thr20 and Glu21 and the C-terminal β-barrel. Within the conserved fold of trypsin-like zymogens, pro-chymase exhibits a zymogen conformation distinct from that of previously studied enzymes.

ACKNOWLEDGMENT

This work is based upon research conducted at the Stanford Synchrotron Radiation Laboratory (SSRL), which is funded by the Department of Energy (BES, BER) and the National Institutes of Health (NCRR, NIGMS).

REFERENCES

1. Schechter, I., and Berger, A. (1967) *Biochem. Biophys. Res. Commun. 27*, 157−162.
2. Caughey, G. H., Zerweck, E. H., and Vanderslice, P. (1991) *J. Biol. Chem. 266*, 12956−12963.
3. Salvesen, G., Farley, D., Shuman, J., Przybyla, A., Reilly, C., and Travis, J. (1987) *Biochemistry 26*, 2289−2293.
4. Jenne, D. E., Masson, D., Zimmer, M., Haefliger, J. A., Li, W. H., and Tschopp, J. (1989) *Biochemistry 28*, 7953−7961.
5. Stroud, R. M., Kossiakoff, A. A., and Chambers, J. L. (1977) *Annu. Rev. Biophys. Bioeng. 6*, 177−193.
6. Wolters, P. J., Pham, C. T., Muilenburg, D. J., Ley, T. J., and Caughey, G. H. (2001) *J. Biol. Chem. 276*, 18551−18556.
7. Khan, A. R., and James, M. N. (1998) *Protein Sci. 7*, 815−836.
8. Freer, S. T., Kraut, J., Robertus, J. D., Wright, H. T., and Xuong, N. H. (1970) *Biochemistry 9*, 1997−2009.
9. Wang, D., Bode, W., and Huber, R. (1985) *J. Mol. Biol. 185*, 595−624.
10. Kossiakoff, A. A., Chambers, J. L., Kay, L. M., and Stroud, R. M. (1977) *Biochemistry 16*, 654−664.
11. Fehlhammer, H., Bode, W., and Huber, R. (1977) *J. Mol. Biol. 111*, 415−438.
12. Pasternak, A., White, A., Jeffery, C. J., Medina, N., Cahoon, M., Ringe, D., and Hedstrom, L. (2001) *Protein Sci. 10*, 1331−1342.
13. Balcells, E., Meng, Q. C., Johnson, W. H., Jr., Oparil, S., and Dell'Italia, L. J. (1997) *Am. J. Physiol. 273*, H1769−H1774.
14. Dell'Italia, L. J., Meng, Q. C., Balcells, E., Wei, C. C., Palmer, R., Hageman, G. R., Durand, J., Hankes, G. H., and Oparil, S. (1997) *J. Clin. Invest. 100*, 253−258.
15. Wei, C. C., Meng, Q. C., Palmer, R., Hageman, G. R., Durand, J., Bradley, W. E., Farrell, D. M., Hankes, G. H., Oparil, S., and Dell'Italia, L. J. (1999) *Circulation 99*, 2583−2589.
16. Hoit, B. D., Shao, Y., Kinoshita, A., Gabel, M., Husain, A., and Walsh, R. A. (1995) *J. Clin. Invest. 95*, 1519−1527.
17. Shiota, N., Okunishi, H., Fukamizu, A., Sakonjo, H., Kikumori, M., Nishimura, T., Nakagawa, T., Murakami, K., and Miyazaki, M. (1993) *FEBS Lett. 323*, 239−242.
18. Shiota, N., Okunishi, H., Takai, S., Mikoshiba, I., Sakonjo, H., Shibata, N., and Miyazaki, M. (1999) *Circulation 99*, 1084−1090.
19. Shiota, N., Jin, D., Takai, S., Kawamura, T., Koyama, M., Nakamura, N., and Miyazaki, M. (1997) *FEBS Lett. 406*, 301−304.
20. Guo, C., Ju, H., Leung, D., Massaeli, H., Shi, M., and Rabinovitch, M. (2001) *J. Clin. Invest. 107*, 703−715.
21. Ju, H., Gros, R., You, X., Tsang, S., Husain, M., and Rabinovitch, M. (2001) *Proc. Natl. Acad. Sci. U.S.A. 98*, 7469−7474.
22. Caughey, G. H., Raymond, W. W., and Wolters, P. J. (2000) *Biochim. Biophys. Acta 1480*, 245−257.
23. Otwinowski, Z., and Minor, W. (1997) in *Macromolecular Crystallography* (Carter, C. W., and Sweet, R. M., Eds.) Part A, pp 307−326, Academic Press, New York.
24. McGrath, M. E., Mirzadegan, T., and Schmidt, B. F. (1997) *Biochemistry 36*, 14318−14324.
25. Navaza, J. (1994) *Acta Crystallogr. A50*, 157−163.
26. CCP4 (1994) *Acta Crystallogr.*, 760−763.
27. Brunger, A. T., Adams, P. D., Clore, G. M., DeLano, W. L., Gros, P., Grosse-Kunstleve, R. W., Jiang, J. S., Kuszewski, J., Nilges, M., Pannu, N. S., Read, R. J., Rice, L. M., Simonson, T., and Warren, G. L. (1998) *Acta Crystallogr., Sect. D 54*, 905−921.
28. Muller, K., Amman, H. J., Doran, D. M., Gerber, P. R., Gubernator, K., and Schrepfer, G. (1988) *Bull. Soc. Chim. Belg. 97*, 655−667.
29. Murshudov, G. N., Vagin, A. A., Lebedev, A., Wilson, K. S., and Dodson, E. J. (1999) *Acta Crystallogr., Sect. D 55*, 247−255.
30. Kleywegt, G. J., and Jones, T. A. (1994) *ESF/CCP4 Newsl.*, 9−14.
31. Pereira, P. J., Wang, Z. M., Rubin, H., Huber, R., Bode, W., Schechter, N. M., and Strobl, S. (1999) *J. Mol. Bio.l 286*, 163−173.
32. Liang, J., Edelsbrunner, H., and Woodward, C. (1998) *Protein Sci. 7*, 1884−1897.
33. Bode, W. (1979) *J. Mol. Biol. 127*, 357−374.
34. Madison, E. L., Kobe, A., Gething, M. J., Sambrook, J. F., and Goldsmith, E. J. (1993) *Science 262*, 419−421.
35. Roach, J. C., Wang, K., Gan, L., and Hood, L. (1997) *J. Mol. Evol. 45*, 640−652.
36. Rotonda, J., Garcia-Calvo, M., Bull, H. G., Geissler, W. M., McKeever, B. M., Willoughby, C. A., Thornberry, N. A., and Becker, J. W. (2001) *Chem. Biol. 8*, 357−368.
37. Waugh, S. M., Harris, J. L., Fletterick, R., and Craik, C. S. (2000) *Nat. Struct. Biol. 7*, 762−765.
38. Hof, P., Mayr, I., Huber, R., Korzus, E., Potempa, J., Travis, J., Powers, J. C., and Bode, W. (1996) *EMBO J. 15*, 5481−5491.
39. Bode, W., Walter, J., Huber, R., Wenzel, H. R., and Tschesche, H. (1984) *Eur. J. Biochem. 144*, 185−190.
40. Hecht, H. J., Szardenings, M., Collins, J., and Schomburg, D. (1991) *J. Mol. Biol. 220*, 711−722.
41. Hedstrom, L., Lin, T. Y., and Fast, W. (1996) *Biochemistry 35*, 4515−4523.
42. Murakami, M., Karnik, S. S., and Husain, A. (1995) *J. Biol. Chem. 270*, 2218−2223.
43. McEuen, A. R., Ashworth, D. M., and Walls, A. F. (1998) *Eur. J. Biochem. 253*, 300−308.
44. McEuen, A. R., Gaca, M. D., Buckley, M. G., He, S., Gore, M. G., and Walls, A. F. (1998) *Eur. J. Biochem. 256*, 461−470.
45. Kaplan, W., and Littlejohn, T. G. (2001) *Briefings Bioinf. 2*, 195−197.
46. Turk, D., Janjic, V., Stern, I., Podobnik, M., Lamba, D., Dahl, S. W., Lauritzen, C., Pedersen, J., Turk, V., and Turk, B. (2001) *EMBO J. 20*, 6570−6582.

BI020594D